

# Intracellular Fate of Polymer Therapeutics Investigated by Fluorescence Lifetime Imaging and Fluorescence Pattern Analysis

J. PANEK<sup>1</sup>, E. KOZIOLOVA<sup>1</sup>, P. STEPANEK<sup>1</sup>, T. ETRYCH<sup>1</sup>, O. JANOUSKOVA<sup>1</sup>

<sup>1</sup>Institute of Macromolecular Chemistry of the Czech Academy of Sciences, Prague, Czech Republic

Received July 14, 2016

Accepted July 14, 2016

## Summary

Nanocarriers bearing anticancer drugs are promising candidates to improve the efficacy of cancer therapy and minimize side effects. The most potent cytostatics used in the treatment of various cancers are anthracyclines, e.g. doxorubicin or pirarubicin. Recently, polymer therapeutics carrying anthracyclines have been intensively studied. The precise characterization of *in vitro* nanocarrier biological behavior brings a better understanding of the nanocarrier characteristics and enables prediction of the behavior of the nanocarrier during *in vivo* application. Advanced fluorescence detection methods, e.g. fluorescence lifetime imaging microscopy (FLIM), were successfully exploited to describe the properties of various polymeric nano-systems and contributed to a complex view of anthracyclines' intracellular transport and DNA intercalation. Here, we report the application of a specific technique for processing FLIM images, called fluorescence pattern decomposition, to evaluate early events after doxorubicin or pirarubicin treatment of cells. Moreover, we characterized changes in the intracellular localization and release of the anthracyclines during the incubation of cells with polymer nanotherapeutics based on poly[N-(2-hydroxypropyl)-methacrylamide] (pHPMA).

## Key words

Therapeutics • Polymer • Anthracycline • Confocal laser scanning microscopy • FLIM • Pattern matching

## Corresponding author

O. Janouskova, Institute of Macromolecular Chemistry of the Czech Academy of Sciences, Heyrovského nám. 2, 162 06 Prague 6, Czech Republic. E-mail: janouskova@imc.cas.cz

## Introduction

Macromolecular and supramolecular systems are being extensively studied as promising candidates in the development of novel therapeutics. Macromolecular carriers with bound or incorporated drugs, e.g. soluble polymers, micelles, polymer-coated liposomes and nanoparticles, have attracted special attention for offering significant improvements in the delivery of anticancer therapeutics (Goldberg *et al.* 2007, Farokhzad and Langer 2009, Mukherjee 2013). They can prolong the circulation time of drugs in the blood stream and greatly decrease drug clearance by increasing molecular weight. Most frequently, polymer nanocarriers are designed to liberate the drug *via* controlled release, which is based on pH-sensitivity, reduction or enzymatic degradation. Such polymer nanotherapeutics improve the drug pharmacokinetics, avoid systemic toxicity and basically promote efficient cellular uptake and preferential subcellular trafficking.

One of the most potent categories of cytostatics, which are successfully used in treatment of various cancers, is the anthracyclines. However, similarly to many other anticancer compounds, their administration can lead to serious side effects, e.g. cardiomyopathy and congestive heart failure. The most famous anthracycline drug is doxorubicin (Dox). To date, several new anthracyclines, e.g. epirubicin (Epi) and pirarubicin (Thp), with enhanced antitumor activity and improved pharmacological profiles have been synthesized and introduced into clinical practice (Minotti *et al.* 2004).

Numerous nanocarriers bearing physically entrapped anthracyclines have been prepared, synthesized

and tested *in vitro* and *in vivo*, e.g. polymer-coated liposomes (Goren *et al.* 2000, Li *et al.* 2009); micelle-forming block copolymers (Yokoyama *et al.* 1990); and nanoparticles (Janes *et al.* 2001, Jin *et al.* 2012). In comparison to nanocarriers with physically entrapped drugs, nanocarriers with the anthracycline covalently attached *via* a spacer that is degradable in the tumor tissue or cell can decrease drug leakage from the carrier during blood transportation and facilitate drug release at the target site (Etrych *et al.* 2011). The carrier structure can be based on water-soluble and biocompatible polymers, e.g. copolymers of N-(2-hydroxypropyl)-methacrylamide (HPMA) (Etrych *et al.* 2001) or polyethylene glycol (PEG) (Rodrigues *et al.* 1999), proteins (Kratz *et al.* 1998) and synthetic polypeptides (Dreher *et al.* 2003).

Advanced fluorescence detection methods – especially fluorescence lifetime imaging microscopy (FLIM) and fluorescence lifetime correlation spectroscopy (FLCS) – can be used for the detailed analysis of the biological behavior of certain nanotherapeutics due to their intrinsic fluorescence. These methods are applicable for evaluating the drug release profile, localization, trafficking, changes in pH, local viscosity and the presence of quencher (Calleja *et al.* 2003, Rihova *et al.* 2010, Lin *et al.* 2003, Clayton *et al.* 2002, Campbell and Uttamchandani 2004). FLIM and FLCS (Dertinger and Rüttinger 2015) have also been used to characterize varied polymeric nano-systems, e.g. to describe DNA interactions with synthetic block copolymers intended for gene delivery (Albuquerque *et al.* 2016), to prove the stability of a glycogen diagnostic nanoprobe in blood plasma (Aasen *et al.* 2015) or to follow the degradation and cargo release from boronate-based polymer nanoparticles with reactive oxygen species (Jäger *et al.* 2016).

The most commonly used of these techniques is FLIM, which produces image contrast based upon the lifetime of the fluorophores. The lifetime of a fluorophore is the average time that the fluorophore remains in the excited state before emitting a fluorescence photon. Interactions between the fluorophore and its local environment can affect the lifetime, which can be exploited to probe the local environment in which the fluorophore resides, e.g. inside the cell. FLIM may serve as a tool to display the distributions of different states of the fluorophore or several fluorophores within the sample as well (Hille *et al.* 2008, Ruedas-Rama *et al.* 2012). FLIM analysis requires fitting an exponential decay

model to individual pixels in the image data, either for selected regions of interest (ROI) or for the whole image. Because the decays of many fluorophores and biomolecules are distinct from simple one-exponential behavior, FLIM image interpretation may become too complex to obtain reasonable results. A more general approach to the analysis of complex FLIM data is searching for specific shapes of fluorescence decay developments, defined as patterns. The computational method called pattern matching or pattern decomposition finds the best linear combination of known (given) decay patterns that represent the data and calculates their relative contributions to the overall decay (Gregor and Patting 2015). This method makes it possible to draw distributions of the patterns even in the case of multi-exponential shape. This feature of pattern decomposition makes the method especially useful for the imaging of fluorophores with complex decay patterns that are typical, e.g. of biomolecules or drugs. Here, we present the use of this to follow the distributions of various chemical states of a polymer drug delivery system within living cells.

## Material and Methods

### *Synthesis of polymer precursor and polymer-drug conjugates*

The HPMA copolymer precursor containing hydrazide groups (pHPMA) was prepared by free radical copolymerization as described previously (Etrych *et al.* 2008). The conjugates pHPMA-Dox and pHPMA-Thp were synthesized by the reaction of the hydrazide groups of pHPMA with the oxo groups of Dox or Thp in methanol in the dark, as described previously (Etrych *et al.* 2008, Nakamura *et al.* 2014). Both polymer conjugates were characterized by size exclusion chromatography with refractive index and MALS detection and by UV-VIS spectrophotometry. The characteristics of the polymer conjugates are described in Table 1.

**Table 1.** Characteristics of polymer conjugates.

| Sample           | M <sub>w</sub><br>(g/mol) | Dispersity | Content<br>of drug<br>(wt%) |
|------------------|---------------------------|------------|-----------------------------|
| <i>pHPMA-Dox</i> | 32,000                    | 1.8        | 8.3                         |
| <i>pHPMA-Thp</i> | 39,000                    | 2.1        | 9.6                         |

### Cell line

The human colorectal adenocarcinoma cell line DLD1 (ATCC, LGC Standards Sp. z.o.o., Poland) was cultivated in RPMI-1640 medium (Life Technology, CR) with heat-inactivated 10 % fetal calf serum (FCS), penicillin (100 U/ml), and streptomycin (100 µg/ml).

### Cell preparation and treatment

DLD1 cells were cultivated for 24 h in 5 % CO<sub>2</sub> at 37 °C on a 35 mm glass bottom dish with 4 chambers, 20 mm microwells, and a#1 cover glass (0.13-0.16 mm) (Bio-Port Europe s.r.o., Czech Republic). The polymer-drug conjugates were dissolved in cultivation medium, and the free drugs were dissolved in DMSO. Then, both the free drugs and the polymer-drug conjugates were added to the corresponding cell lines at a final drug concentration of 1 µg·ml<sup>-1</sup>. After 30 minutes, the cells were washed twice with PBS, and the intracellular fluorescence signal of the drug was detected on an IX83 confocal laser scanning microscope (Olympus, Tokyo, Japan) equipped with a FLIM/FLCS upgrade kit (PicoQuant GmbH, Berlin, Germany).

### Fluorescence Lifetime Imaging Microscopy (FLIM) and Fluorescence Pattern Analysis

The cell samples were excited by an LDH-D-C-485 laser diode emitting 482 nm light, driven by a PDL 828 Sepia II driver in picosecond pulsed mode at a 20 MHz repetition rate (both devices: PicoQuant) through the 488 nm dichroic mirror built into the IX83 scan head. An Olympus UPlanSApo water immersion objective (60x, 1.2 NA) delivered the excitation light into a diffraction-limited spot and collected the emitted fluorescence. The fluorescence signal passed through a Semrock 600/50 nm BrightLine emission filter and was detected by a hybrid photomultiplier (PMA Hybride-40 from PicoQuant) operated in photon counting mode. Photon counts were recorded using a PicoHarp300 TCSPC module in a T3 time tagging mode (Wahl *et al.* 2007). The SymPhoTime64, ver. 2.1 software from PicoQuant was used for data acquisition, FLIM and pattern decomposition analysis. Image acquisition took 5 min, and the measurements were performed at 23±1 °C.

## Results

### Fluorescence decay patterns and lifetimes of Dox and Thp

Two types of cell experiments were performed for both Dox and Thp: i) a control experiment, containing free

drug added directly to the cultivated DLD1 cells at a final drug concentration of 1 µg·ml<sup>-1</sup>; and ii) experiments containing polymer-drug conjugate added at the same final drug concentration of 1 µg·ml<sup>-1</sup>. The data acquisition began after 30 minutes, and FLIM images were acquired for each of the control samples. The typical countrates and photon-numbers/pixel for all the obtained sub-patterns are shown in Table 2. The images were further analyzed by the pattern decomposition method using correlograms of average lifetime  $\tau_{Av}$  against the lifetime distribution  $\sigma_\tau$  (Gregor and Patting 2015) to identify the patterns of a given cell experiment. The decay patterns calculated for the Dox and Thp controls are shown in Figure 1 and Figure 2, respectively. As multiple sub-patterns were detected in all of the control samples, the signal intensities were normalized to allow comparison of the decay development. Free Dox shows 3 decay sub-patterns, free Thp contains 2 sub-patterns, and the polymer-Dox and polymer-Thp conjugates each contain 2 different fluorescence sub-patterns. The sub-patterns are clearly distinguishable from one another. The sub-pattern curve shapes were verified by fitting with exponential functions consisting of 1, 2 or 3 exponential components. The results confirm that the decays are strongly distinct from single exponential decays, as even 3 exponentials do not fit the data perfectly. The overview of the fitted life-times  $\tau_i$  corresponding to 3-component exponential models is summarized in Table 3. The standard FLIM is not applicable for decomposing an image into several decays if each of them is described by 3 or more exponential components. Therefore the pattern matching technique was used to resolve the task and depict sub-pattern distributions in the control samples.

### Distribution of pattern decays

The distributions of the above mentioned sub-patterns over the measured samples are shown in Figure 3 and Figure 4. The artificial colors correspond to the presence of specific sub-patterns, and the brightness of the colors reflects the relative amplitude of the sub-pattern in a given pixel. For free Dox and free Thp, the patterns cover mainly monochrome compact areas, whereas for the polymer-drug conjugates, the color distributions are fuzzier and overlapping, which indicates smaller degree of localization of the decay patterns of the conjugates. This appearance can reflect the different rates of distribution of the free drug as well as the drug release rate from the polymer backbone after a short incubation time.

**Table 2.** Values of the typical countrates observed during measurements of separate samples and values of the typical photon numbers/pixel for individual sub-pattern distributions.

| Sample, pattern    | Typical countrates [kcnts/s] | Intervals of typical photon-numbers/pixel [kcnts] |
|--------------------|------------------------------|---|
| Free Dox, patt. 1  | 140                          | 1.0-2.0   |
| Free Dox, patt. 2  |                              | 0.3-0.7   |
| Free Dox, patt. 3  |                              | 0.5-1.0   |
| pHPMA-Dox, patt. 1 | 30                           | 0.1-0.5   |
| pHPMA-Dox, patt. 2 |                              | 0.5-1.0   |
| Free Thp, patt. 1  | 170                          | 1.0-3.0   |
| Free Thp, patt. 2  |                              | 0.5-1.5   |
| pHPMA-Thp, patt. 1 | 160                          | 1.0-2.5   |
| pHPMA-Thp, patt. 2 |                              | 0.5-1.0   |

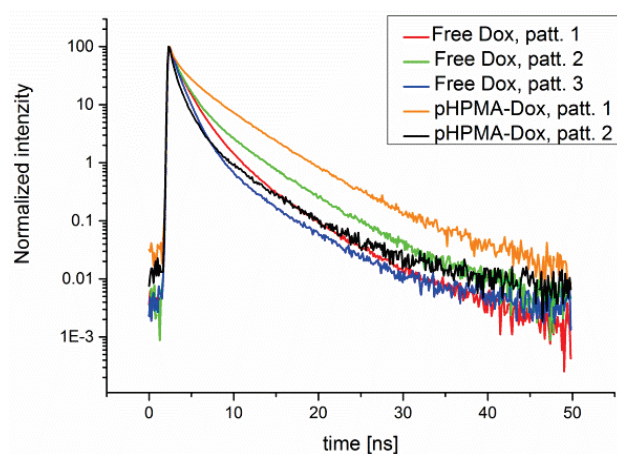


**Fig. 1.** Normalized fluorescence decay patterns extracted from the control samples containing DLD1 cells incubated with **i)** free Dox at a final concentration of  $1 \mu\text{g}\cdot\text{ml}^{-1}$  (Free Dox patterns); **ii)** pHPMA-Dox conjugate at a final Dox concentration of  $1 \mu\text{g}\cdot\text{ml}^{-1}$  (pHPMA-Dox patterns). The data acquisition was performed after ca. 30-minute incubation.

**Table 3.** Lifetimes calculated by fitting the corresponding individual sub-patterns with 3-component exponential models.

| Sample, pattern    | $\tau_1$ [ns] | $\tau_2$ [ns] | $\tau_3$ [ns] |
|--------------------|---------------|---------------|---------------|
| Free Dox, patt. 1  | 1.69          | 0.69          | 4.58          |
| Free Dox, patt. 2  | 1.60          | 0.65          | 4.69          |
| Free Dox, patt. 3  | 1.30          | 0.67          | 4.58          |
| pHPMA-Dox, patt. 1 | 2.36          | 0.58          | 5.11          |
| pHPMA-Dox, patt. 2 | 1.22          | 0.41          | 4.63          |
| Free Thp, patt. 1  | 1.42          | 0.50          | 3.80          |
| Free Thp, patt. 2  | 1.60          | 0.93          | 5.21          |
| pHPMA-Thp, patt. 1 | 1.62          | 0.61          | 4.62          |
| pHPMA-Thp, patt. 2 | 1.79          | 0.71          | 4.84          |

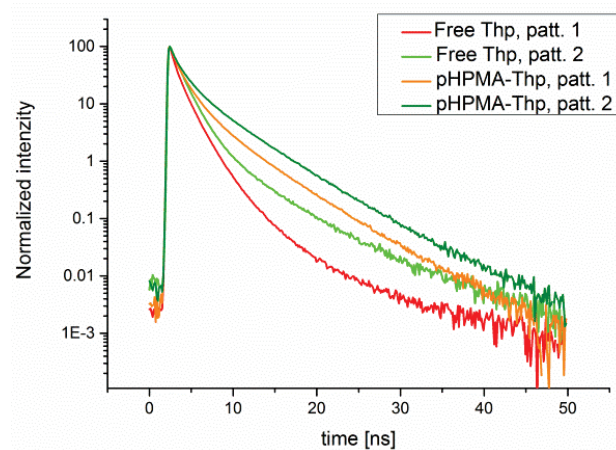


**Fig. 2.** Normalized fluorescence decay patterns extracted from the control samples containing DLD1 cells incubated with **i)** free Thp at a final concentration of  $1 \mu\text{g}\cdot\text{ml}^{-1}$  (Free Thp patterns); **ii)** pHPMA-Thp conjugate at a final Thp concentration of  $1 \mu\text{g}\cdot\text{ml}^{-1}$  (pHPMA-Thp patterns). The data acquisition was performed after ca. 30-minute incubation.

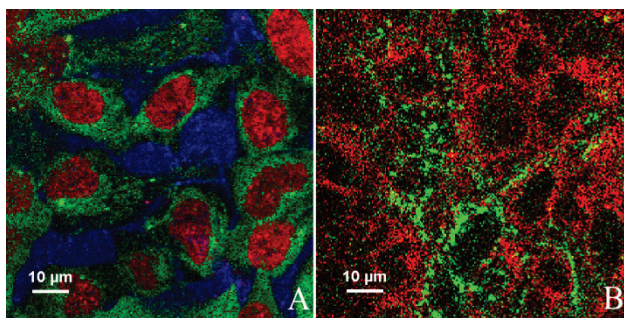


**Fig. 3.** Fluorescence pattern distributions detected after 30-minute incubation of DLD1 cells with initially free Dox (**A**) and pHPMA-Dox conjugate (**B**) in artificial colors. **A**) Red: Free Dox, patt 1; Green: Free Dox, patt 2; Blue: Free Dox, patt 3. **B**) Red: pHPMA-Dox, patt 1; Green: pHPMA-Dox, patt 2.

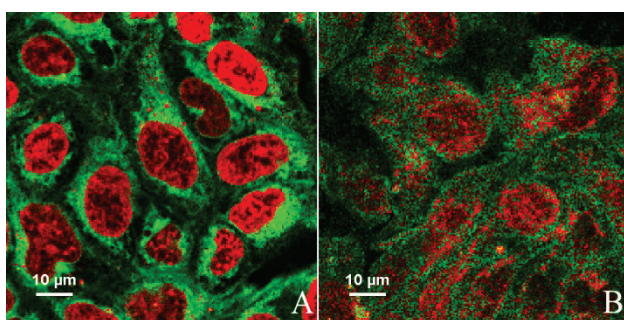


**Fig. 4.** Fluorescence pattern distributions detected after 30-minute incubation of DLD1 cells with initially free Thp (**A**) and pHPMA-Thp conjugate (**B**) in artificial colors. **A**) Red: Free Thp, patt 1; Green: Free Thp, patt 2. **B**) Red: pHPMA-Thp, patt 1; Green: pHPMA-Thp, patt 2.

#### *Distributions of sub-patterns in cells incubated with free Dox and polymer-Dox conjugates*

The distributions of three sub-patterns of free Dox are depicted in Figure 3A. The red pattern (Free Dox, patt. 1) shows the nuclear localization, the green pattern (Free Dox, patt. 2) corresponds to the localization of the free DOX in the cytoplasm around the nucleus, and the blue pattern is localized in the cytoplasm close to the cell membrane. In contrast to free Dox, the pHPMA-Dox conjugate has different pattern distributions, as shown in Figure 3B. The red pattern (pHPMA-Dox; patt 1) is localized predominantly in the cytoplasm, demonstrating a slower rate of internalization of polymer-bound Dox than for the free Dox and the essential need to establish drug release in the endosomes and lysosomes of cells. In other words, the red pattern (pHPMA-Dox, patt. 1) is not related only to the nucleus localization, i.e. to the signal corresponding to intercalation into DNA seen in Figure 3A. The green pattern (pHPMA-Dox; patt 2) is spread mostly around the nucleus in the cytoplasm, but it is less pronounced. The very rare localization of

individual green points in the nucleus is a typical example of detection noise. The brightness of the green color and localization of this pattern refers to the slower internalization of pHPMA bound Dox. No equivalent of the third blue pattern of the free DOX (Free Dox, patt. 3) was detected in the pHPMA-DOX sample.

#### *Distributions of sub-patterns in cells incubated with free Thp and polymer-Thp conjugates*

The signal of the free Thp is decomposed into two sub-patterns within the cells, as illustrated in Figure 4A. The red pattern (Free Thp, patt. 1) corresponds to nuclear localization; the green pattern (Free Thp, patt. 2) corresponds to the localization of free Thp in the cytoplasm around the nucleus. The brightness of the respective colors of both sub-patterns are higher than in the case of free Dox, which highlights the different behavior of these drugs, namely the faster penetration of Thp across the cell membrane. The third sub-pattern was not detected in the sample containing free Thp, which may imply both the Thp different penetration rate in comparison with the free DOX and changes to the Dox molecule in the intracellular environment (Shinozaki *et al.* 2002).

The pattern decomposition for the pHPMA-Thp conjugate is shown in Figure 4B. The two sub-patterns here have similar distributions to the control sample containing free Thp, except that the brightness of the respective colors is lower for the polymer conjugates. The green pattern (pHPMA-Thp, patt. 2) corresponds to the localization of the pHPMA-Thp conjugate in the cytoplasm around the nucleus. The red pattern (pHPMA-Thp, patt. 1) is predominantly localized in the nucleus and partly also in the cytoplasm of the cells, which may document relatively slower internalization of the polymer drug conjugate and subsequent release from the polymer backbone. These observations are discussed further below.

## Discussion

### *Pattern definition*

The key part of pattern decomposition analysis is the proper definition of the pattern decays. The complete set of relevant patterns can be obtained either from control sample measurements or from a mixed (conventional) sample itself. As the latter method often fails for multi-exponential decays, the preparation of control samples is preferred. Moreover, even singly

stained controls may contain more than 1 decay pattern in the FLIM image. Such sub-patterns may often result from the variable microenvironments that surround the fluorophore within the sample (e.g. in different compartments of cells), as hydrophobicity, pH and other factors influence the decay characteristics of many dyes and fluorescent biomolecules. The individual sub-patterns may cover either compact areas or complex spatial distributions across the FLIM image. For compact homogeneous areas containing a single sub-pattern, a Region of Interest (ROI) can be selected in the FLIM image to define the decay pattern corresponding to the ROI. On the other hand, for complicated distributions, it is helpful to represent the FLIM data using two-dimensional diagrams (Gregor and Patting 2015, Niehorster *et al.* 2016). These diagrams show, e.g. the correlation between the average lifetime  $\tau_{Av}$  and the width of the lifetime distribution  $\sigma_\tau$  extracted from every pixel of the FLIM image. Correlograms of  $\tau_{Av}$  against  $\sigma_\tau$ , called also decay diversity maps, are useful for the identification of different states of fluorescent compounds present within the sample. As a single fluorophore (drug) in a specific physicochemical state usually creates a maximum clearly visible as a 2D peak in the decay diversity map, it is possible to select regions that correspond to all relevant sub-patterns. In other words, if the distribution maxima present in 2D-correlograms are distinguishable, the use of the decay diversity map allows the reliable construction of the set of decay patterns. In our experience, anthracycline control samples usually give one or several correlogram peaks that are distinct from one another. Therefore, the controls containing free or polymer-bound drug were measured independently.

#### *Verification of correct pattern definition by pattern matching for the controls*

The quality and correctness of the patterns extracted from the control samples were verified by backward decomposition of their FLIM images. As a cross-check, the data acquired for both free drugs and polymer-drug conjugates were considered to be unknown mixed samples, and all sub-patterns found earlier were included in new pattern matching calculations. The patterns of the free drug showed almost zero (or slightly negative) relative amplitude in the polymer-drug control samples and vice versa. The patterns related to polymer-drug conjugates were not found in the free-drug data files for either Dox or Thp (data not shown). This result demonstrates that the patterns obtained by the pattern

matching technique are not interchangeable. For Thp, the further interpretation is as follows. A fraction of the released Thp was detected in the pHPMA-Thp control, corresponding to a relatively fast release of Thp from the polymer carrier. As shown in Figure 2, the decays of initially free (Free Thp, patt. 1) and just-released Thp (pHPMA-Thp, patt. 1) are distinct, even though they correspond to similar localizations. This difference can be explained by changes in the excitation state of the initially free and freshly released Thp molecules, as well as to the various pathways for their internalization into the nucleus.

#### *Identification of free and bound drugs by pattern matching*

Using the pattern matching evaluation, we can monitor the differences in the localization of the free drugs, drugs just released from the polymer backbone and polymer-drug conjugates.

In contrast to free Dox, free Thp shows different pattern components, which may correspond to the faster uptake of Thp across the cell membrane and different interactions with the intracellular microenvironment. The representation of patterns across the samples incubated with the polymer-drug conjugates shows different distributions than for free drugs. For pHPMA-DOX, no pattern component is localized in the nucleus, only outside in the cytoplasm. This observation documents both the slower trafficking of released Dox to the nucleus compared to Thp and the rapid trafficking of Thp released outside the cells during incubation. The pHPMA-Thp pattern components were present in both the nucleus and the cytoplasm. In Figure 4B, the red sub-pattern - present mainly in the nucleus - is also partly localized around the cytoplasm, but it shows much less sharp spatial distributions than the red sub-pattern of the initially free Thp from the first control sample (Free Thp, patt 1). The sub-pattern (pHPMA-Thp, patt 1) is most likely related to a specific physicochemical state of the Thp molecule that gradually becomes concentrated in the nucleus.

The pattern-matching calculations using the whole set of Thp sub-patterns confirm not only the ability to identify free and bound anthracycline drug in the FLIM image but also the ability to distinguish between the patterns of originally free Thp added to the cells and Thp released from conjugation with the polymer. Standard FLIM was also tested for that purpose, but the results were not satisfactory, as the auto-fluorescence decays of the anthracycline drugs are complex and very different

from single-exponential decay. Moreover, the dependence of the fluorescence decay on the chemical state is clearly different for free and bound drugs, which makes the task even more demanding. The pattern decomposition method decreases the number of unknown parameters because it does not include an analytical description of each decay curve, and therefore it can extract different states of the anthracycline drugs in the sample.

## Conclusions

In summary, a numerical pattern decomposition method was used to distinguish the free and pHPMA-bound anthracycline drugs Dox and Thp within living cells, and the technique was applied to follow drug

distributions and monitor the early fate of the pHPMA-drug delivery systems in the cells. The potential to characterize changes in cells after treatment with cancerostatics was clearly demonstrated, opening up new opportunities to fill in detailed information on the behavior of nanotherapeutics inside cells.

## Conflict of Interest

There is no conflict of interest.

## Acknowledgements

This work was supported by the Ministry of Education, Youth and Sports of CR within the National Sustainability Program I (NPU I), Project POLYMAT LO1507.

## References

- AASEN SN, POSPISILOVA A, EICHLER TW, PANEK J, HRUBY M, STEPANEK P, SPRIET E, JIRAK D, SKAFTNESMO KO, THORSEN F: A novel nanoprobe for multimodal imaging is effectively incorporated into human melanoma metastatic cell lines. *Int J Mol Sci* **16**: 21658-21680, 2015.
- ALBUQUERQUE LJC, ANNES K, MILAZZOTTO MP, MATTEI B, RISKE KA, JAGER E, PANEK J, STEPANEK P, KAPUSTA P, MURARO PIR, DE FREITAS AGO, SCHMIDT V, GIACOMELLI C, BONVENT JJ, GIACOMELLI FC: Efficient condensation of DNA into environmentally responsive polyplexes produced from block cationomers carrying amine or diamine groups. *Langmuir* **32**: 577-586, 2016.
- CALLEJA V, AMEER-BEG SM, VOJNOVIC B, WOSCHOLSKI R, DOWNWARD J, LARIJANI B: Monitoring conformational changes of proteins in cells by fluorescence lifetime imaging microscopy. *Biochem J* **372**: 33-40, 2003.
- CAMPBELL A, UTTAMCHANDANI D: Optical dissolved oxygen lifetime sensor based on sol-gel immobilisation. *IEE Proc Sci Meas Technol* **151**: 291-297, 2004.
- CLAYTON AH, HANLEY QS, ARNDT-JOVIN DJ, SUBRAMANIAM V, JOVIN TM: Dynamic fluorescence anisotropy imaging microscopy in the frequency domain (rFLIM). *Biophys J* **83**: 1631-1649, 2002.
- DERTINGER T, RÜTTINGER S: Advanced FCS: An introduction to fluorescence lifetime correlation spectroscopy and dual-focus FCS. In: *Advanced Photon Counting: Applications, Methods, Instrumentation*. KAPUSTA P, WAHL M, ERDMANN R (eds), Springer International Publishing, Cham, 2015, pp 89-109.
- DREHER MR, RAUCHER D, BALU N, MICHAEL COLVIN O, LUDEMAN SM, CHILKOTI A: Evaluation of an elastin-like polypeptide-doxorubicin conjugate for cancer therapy. *J Control Release* **91**: 31-43, 2003.
- ETRYCH T, CHYTIL P, MRKVAN T, SIROVA M, RIHOVA B, ULBRICH K: Conjugates of doxorubicin with graft HPMA copolymers for passive tumor targeting. *J Control Release* **132**: 184-192, 2008.
- ETRYCH T, JELINKOVA M, RIHOVA B, ULBRICH K: New HPMA copolymers containing doxorubicin bound via pH-sensitive linkage: synthesis and preliminary in vitro and in vivo biological properties. *J Control Release* **73**: 89-102, 2001.
- ETRYCH T, KOVAR L, STROHALM J, CHYTIL P, RIHOVA B, ULBRICH K: Biodegradable star HPMA polymer-drug conjugates: Biodegradability, distribution and anti-tumor efficacy. *J Control Release* **154**: 241-248, 2011.
- FAROKHZAD OC, LANGER R: Impact of nanotechnology on drug delivery. *ACS Nano* **3**: 16-20, 2009.
- GOLDBERG M, LANGER R, JIA X: Nanostructured materials for applications in drug delivery and tissue engineering. *J Biomater Sci Polym Ed* **18**: 241-268, 2007.

- GOREN D, HOROWITZ AT, TZEMACH D, TARSHISH M, ZALIPSKY S, GABIZON A: Nuclear delivery of doxorubicin via folate-targeted liposomes with bypass of multidrug-resistance efflux pump. *Clin Cancer Res* **6**: 1949-1957, 2000.
- GREGOR I, PATTING M: Pattern-based linear unmixing for efficient and reliable analysis of multicomponent TCSPC data. In: *Advanced Photon Counting: Applications, Methods, Instrumentation*. KAPUSTA P, WAHL M, ERDMANN R (eds), Springer International Publishing, Cham, 2015, pp 241-263.
- HILLE C, BERG M, BRESSEL L, MUNZKE D, PRIMUS P, LOHMANNROBEN HG, DOSCHE C: Time-domain fluorescence lifetime imaging for intracellular pH sensing in living tissues. *Anal Bioanal Chem* **391**: 1871-1879, 2008.
- JAGER E, HOCHERL A, JANOUSKOVA O, JAGER A, HRUBY M, KONEFAL R, NETOPILIK M, PANEK J, SLOUF M, ULBRICH K, STEPANEK P: Fluorescent boronate-based polymer nanoparticles with reactive oxygen species (ROS)-triggered cargo release for drug-delivery applications. *Nanoscale* **8**: 6958-6963, 2016.
- JANES KA, FRESNEAU MP, MARAZUELA A, FABRA A, ALONSO MJ: Chitosan nanoparticles as delivery systems for doxorubicin. *J Control Release* **73**: 255-267, 2001.
- JIN YH, HU HY, QIAO MX, ZHU J, QI JW, HU CJ, ZHANG Q, CHEN DW: pH-sensitive chitosan-derived nanoparticles as doxorubicin carriers for effective anti-tumor activity: preparation and in vitro evaluation. *Colloids Surf B Biointerfaces* **94**: 184-191, 2012.
- KRATZ F, BEYER U, ROTH T, TARASOVA N, COLLERY P, LECHENAULT F, CAZABAT A, SCHUMACHER P, UNGER C, FALKEN U: Transferrin conjugates of doxorubicin: synthesis, characterization, cellular uptake, and in vitro efficacy. *J Pharm Sci* **87**: 338-346, 1998.
- LI X, DING L, XU Y, WANG Y, PING Q: Targeted delivery of doxorubicin using stealth liposomes modified with transferrin. *Int J Pharm* **373**: 116-123, 2009.
- LIN HJ, HERMAN P, LAKOWICZ JR: Fluorescence lifetime-resolved pH imaging of living cells. *Cytometry A* **52**: 77-89, 2003.
- MINOTTI G, MENNA P, SALVATORELLI E, CAIRO G, GIANNI L: Anthracyclines: molecular advances and pharmacologic developments in antitumor activity and cardiotoxicity. *Pharmacol Rev* **56**: 185-229, 2004.
- MUKHERJEE B: Nanosize drug delivery system. *Curr Pharm Biotechnol* **14**: 1221, 2013.
- NAKAMURA H, ETRYCH T, CHYTIL P, OHKUBO M, FANG J, ULBRICH K, MAEDA H: Two step mechanisms of tumor selective delivery of N-(2-hydroxypropyl)methacrylamide copolymer conjugated with pirarubicin via an acid-cleavable linkage. *J Control Release* **174**: 81-87, 2014.
- NIEHORSTER T, LOSCHBERGER A, GREGOR I, KRAMER B, RAHN HJ, PATTING M, KOBERLING F, ENDERLEIN J, SAUER M: Multi-target spectrally resolved fluorescence lifetime imaging microscopy. *Nat Methods* **13**: 257-262, 2016.
- RIHOVA B, ETRYCH T, SIROVA M, KOVAR L, HOVORKA O, KOVAR M, BENDA A, ULBRICH K: Synergistic action of doxorubicin bound to the polymeric carrier based on N-(2-hydroxypropyl)methacrylamide copolymers through an amide or hydrazone bond. *Mol Pharm* **7**: 1027-1040, 2010.
- RODRIGUES PC, BEYER U, SCHUMACHER P, ROTH T, FIEBIG HH, UNGER C, MESSORI L, ORIOLI P, PAPER DH, MULHAUPT R, KRATZ F: Acid-sensitive polyethylene glycol conjugates of doxorubicin: preparation, in vitro efficacy and intracellular distribution. *Bioorg Med Chem* **7**: 2517-2524, 1999.
- RUEDAS-RAMA MJ, ORTE A, HALL EAH, ALVAREZ-PEZ JM, TALAVERA EM: A chloride ion nanosensor for time-resolved fluorimetry and fluorescence lifetime imaging. *Analyst* **137**: 1500-1508, 2012.
- SHINOZAKI T, WATANABE H, YANAGAWA T, SHIRAKURA K, TAKAGISHI K: Pirarubicin-based versus doxorubicin-based osteosarcoma chemotherapy. *Ann Pharmacother* **36**: 996-999, 2002.
- WAHL M, RAHN HJ, GREGOR I, ERDMANN R, ENDERLEIN J: Dead-time optimized time-correlated photon counting instrument with synchronized, independent timing channels. *Rev Sci Instrum* **78**: 033106, 2007.
- YOKOYAMA M, MIYAUCHI M, YAMADA N, OKANO T, SAKURAI Y, KATAOKA K, INOUE S: Characterization and anticancer activity of the micelle-forming polymeric anticancer drug adriamycin-conjugated poly(ethylene glycol)-poly(aspartic acid) block copolymer. *Cancer Res* **50**: 1693-1700, 1990.